Polarity crossover regions of transient earth fault relays in non-radial resonant grounded networks☆,☆☆

Thomas Treider *, Hans Kristian Høidalen

Department of Electric Power Engineering, Norwegian University of Science and Technology, Trondheim, Norway

ABSTRACT

Transient-based earth fault protection is widely used in all types of resonant grounded networks, and though the operating principles of the commonly available relays are usually derived from radial networks, manufacturers claim applicability in meshed networks as well. This paper utilizes a laboratory setup to study the directional indication of four transient earth fault relays in non-radial resonant grounded networks. Two of the relays considered are widely used analog single-purpose transient earth fault relays, whereas the other two relays represent two transient-based earth fault functions found in modern protective devices. The paper verifies the location of crossover points according to the presented theory, i.e. fault locations for which relays transition between seeing faults as forward and reverse faults, and demonstrates the viability of the proposed theoretical analysis of crossover points. However, presented analytical formulae only describe the two analog relays accurately, whereas the two modern relays have a more complex operating principle which requires further analysis to quantify properly. Finally, it is shown that relay misoperation which is not easily fixed by communication between relays can occur, and it is suggested that network operators conduct detailed relay coordination when applying transient earth fault relays instead of relying on standardized settings.

1. Introduction

Throughout Europe and Asia, MV and HV distribution systems are commonly resonant grounded. In this system earthing scheme, an inductor is placed between the transformer neutral and ground in one or several transformers in the network. These inductors are often referred to as Petersen coils, though Arc Suppression Coils (ASCs) is a more precise general term. During single phase faults, usually referred to as earth faults or ground faults in these systems, the capacitive part of the fault current is largely canceled out by the inductive current introduced by the ASCs in the system. As a result, with correctly tuned ASCs, the fault current can be brought to a minimum, leading to self-extinguishing arcing faults. This property leads to automatic clearing of many single phase faults, and due to the small fault current the permanent earth faults can be allowed to be present in the system for longer time periods and thus giving network operators time to move loads to other feeders and limit the number of affected customers. Resonant grounded networks thus have few interruptions and a high quality of supply, but the low fault current level also introduces significant challenges for protection systems. As the fault current can be in the same order of magnitude as the normal load currents, or even smaller,

conventional over-current protection or distance protection cannot be applied.

In distribution systems, which have traditionally been radially operated, the earth fault protection system is often based on zero-sequence currents and voltage. As no reliable distance element has existed for earth faults in resonant grounded systems, the protection system is often limited to determining the faulty feeder using directional elements. Measuring the current and voltage, a directional element can be realized in a number of ways to identify the faulty feeder [1]. Some network operators utilize several measurement points along the feeder to narrow down the faulty section using fault passage indicators [2], but precise fault location is still a much more challenging exercise in these networks. Furthermore, to get reliable operation of the protection systems, a resistor is often required to be connected in parallel with the ASC to produce a significantly large watt-metric component for the protection systems to detect [3].

Quite a few different protection principles based on the relationship between voltage and currents in the zero-sequence system have been devised, but they are largely based on the assumption of a radial system for the directional element to work properly [4–8]. Some recent works

have presented novel algorithms and techniques which may be suited for meshed networks as well. The EDIST-method [9,10] introduces a transient-based distance element, remedying an important limitation often seen in transient-based protection which is the lack of any information pertaining to distance. In Refs. [11,12] a transient principle is proposed to serve as a directional element, and a communication system is used to implement a permissive overreach transfer trip scheme in order to ensure correct operation in a meshed network.

In the future, more distribution networks may be operated with some degree of meshing or ring-connection of feeders to increase the quality of supply and better integrate distributed generation [13]. Furthermore, the regional networks, the intermediate network level sitting between the distribution system and the transmission system, is often resonant grounded. These networks resemble transmission systems in terms of their topology, with larger meshes and often several power transformers and ASCs present in the system. In these networks the only option for directional earth fault indication has been what is broadly referred to as transient earth fault protection. Traditionally, this term has referred to a few analog relays based on a similar principle of operation utilizing the high frequency transients that occurs during earth faults [14,15]. In recent years modern protective relays have become equipped with more advanced functions based on these transients, such as [16,17], so the transient protection category is now more diverse.

Although many of the commonly used transient-based earth fault relays, hereafter referred to as Transient Earth Fault Relays (TEFRs), are said to be valid in non-radial networks [14–17], it is not well established whether or not they have some inherent limitations in such networks compared to radially operated networks. The availability of relay testing in the scientific literature is limited mainly to sparse results from tests conducted by relay manufacturers, and independent research papers studying their performance in detail is lacking. Furthermore, the TEFR-category is actually quite diverse, and it is not unlikely that previous generations of relays with a less reliable performance have been allowed to define a broad category of relays.

This paper therefore has two primary objectives. The first is to identify and investigate any inherent limitations for network operators to be aware of when applying TEFRs in non-radial networks. To do this, the paper focuses on studying the fault direction indication in non-radial networks and the transition between forward and reverse faults. Secondly, the paper aims to identify any variation in the responses of different TEFRs to determine how the various operating principles differ from each other. The paper will build on the theoretical analysis performed in [18] and investigate the performance of four different relays. These four relays are then tested in a laboratory setup with a variation of network configurations and parameters.

The rest of the paper is organized as follows. Section 2 briefly explains the theoretical foundation for the earth fault transients and discusses some potential issues related to sensitivity and polarity. Based on this theory, formulae are provided which predict the fault locations for which the relays will transition between forward and reverse fault indication. Section 3 describes the simulation models and the laboratory setup used to test the relays, whereas the results are discussed and analyzed in detail in Section 4. Section 5 discusses the impact of various parameters in the tests, and the validity and limitations of the laboratory tests are also discussed in detail. Finally, conclusions and recommendations for future work is provided in Section 6.

2. Earth fault transients in non-radial networks

A detailed presentation of important theoretical concepts was given in Ref. [18], but the key concepts required to discuss the results in this paper are repeated in this section. This section primarily deals with the earth fault transients in a non-radial system, and for more details on the charging transient and its behavior in radial networks interested readers are referred to [18] for further reading.
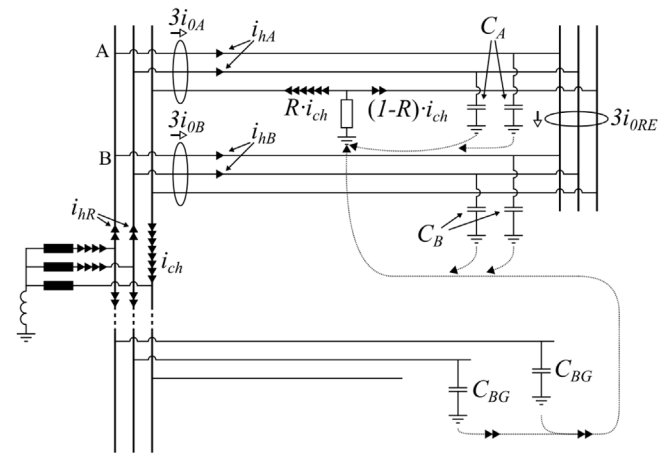

Fig. 1. Charging transient in a ring-operated network.

2.1. The charging transient

Note that the equations derived in this section apply at the charging transient frequency only.

During an earth fault in a network with isolated or compensated grounding, the phase-ground voltages of the two healthy phases increase. This charging process is associated with what is commonly referred to as the charging transient, which is described as a current flowing from the faulted point along the faulted phase until it reaches the main transformer neutral. Here, it is divided in two equal parts and returning to the fault point via the healthy phase capacitances. In this path the transformer leakage inductance and the faulty phase series inductance make up to main inductance L_{eq}, whereas the healthy phase capacitances to ground and to the faulted phase make up the main capacitance C_{eq}. The charging current thus flows in some equivalent LC-circuit with a natural frequency given by (1).

$$f = \frac{1}{2\pi\sqrt{L_{eq}C_{eq}}} \tag{1}$$

Different versions of this model are available in the literature, differing slightly from each other in how the equivalent inductance L_{eq} and capacitance C_{eq} of the circuit are approximated [9,19,20].

Consider a fault taking place somewhere on line A in Fig. 1. The charging transient i_{ch} flows along the faulted phase to the transformer neutral and returns to ground via the healthy phase capacitances. As the two lines A and B are connected to form a ring, the charging transient will have two alternative paths along the faulted phase to the main transformer. The division of i_{ch} is based on the impedance of the faulted phase, and the ratio can be obtained by applying the current division principle. This ratio is defined as R, such that the current $R \cdot i_{ch}$ flows towards the transformer neutral along line A, whereas $(1 - R) \cdot i_{ch}$ flows towards the transformer neutral along line B. The charging current reaches the transformer neutral where it is divided in two halves, assuming the two healthy phases to be identical. The current then returns to the faulted point via the capacitances of the healthy phases, as indicated in Fig. 1. In Fig. 1, the capacitances C_A and C_B are the per phase capacitances on line A and B, whereas C_{BG} is the total per phase capacitance of the background network, represented here as a single feeder.

Because $\frac{1}{2}i_{ch}$ returns to ground in each of the healthy phases in the network as a whole, the component that returns on the ring itself, denoted i_{hR} in Fig. 1, is given by (2).
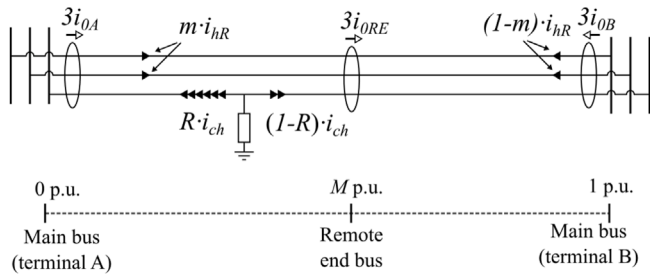
$$i_{hR} = \frac{1}{2}i_{ch}\frac{C_R}{C_T} \tag{2}$$

Fig. 2. Remote end bus measurement on a network ring.

Fig. 3. Test network for investigating location of crossover points.

In (2), $C_R = C_A + C_B$ is the total per phase capacitance of the ring, whereas $C_T = C_R + C_{BG}$ is the total per phase capacitance of the entire network. Eq. (2) shows that it is the amount of capacitance on the ring compared the background network which determines how much of i_{ch} returns on the ring itself. Depending on the parameters of the two feeders in the ring, the current i_{hR} will divide itself among lines A and B. Let this be described by the factor m, such that the currents

$$i_{hA} = m \cdot i_{hR}$$
$$i_{hB} = (1 - m) \cdot i_{hR} \tag{3}$$

flow onto line A and line B, respectively. In the case of a homogeneous ring, the division of i_{hR} will be equal among the two lines (i.e., $m = 0.5$). In any case, m is determined by the network topology and it is independent of the fault location.

The charging transient frequency component of the residual current measured on lines A and B can be written as

$$3i_{0A} = 2i_{hA} - R \cdot i_{ch}$$
$$3i_{0B} = 2i_{hB} - (1 - R) \cdot i_{ch} \tag{4}$$

Combining (2), (3) and (4), (5) is obtained.

$$3i_{0A} = i_{ch} \left(m \frac{C_R}{C_T} - R \right)$$
$$3i_{0B} = i_{ch} \left((1 - m) \frac{C_R}{C_T} - (1 - R) \right) \tag{5}$$

Similarly, the measured current $3i_{0RE}$ at the remote end bus bar on the ring can also be derived. With the measurement polarity as shown in Fig. 1, this current is expressed as a function of the fault location as well as the location of the remote end bus itself on the ring. Fig. 2 illustrates this way of measuring the distance by drawing the ring AB as a straight feeder. Note how both ends of the figure correspond to the main bus. The per unit distance around the ring is measured along the ring in a clockwise direction starting on line A, and the distance to the remote end bus is denoted M. Then, a remote end bus would for instance be located at $M = 0.5$ p.u. in the case of two lines of the same length, or at $M = 0.67$ p.u. in the case of line A being twice as long as line B. It can then be shown that the current $3i_{0RE}$ is given by (6).

$$3i_{0RE} = i_{ch} \left(\frac{C_R}{C_T} (m - M) + 1 - R \right) \tag{6}$$

Eq. (5) and (6) describe the charging current measured at the three measurement locations shown in Fig. 1, and they apply for this particular topology. Note that the presence of loads on the ring, either at bus M or on branches connected to the feeders A and B, will not significantly impact these results as load transformers represent a much higher impedance path for the transient than the path indicated in Fig. 1.

2.2. Crossover points

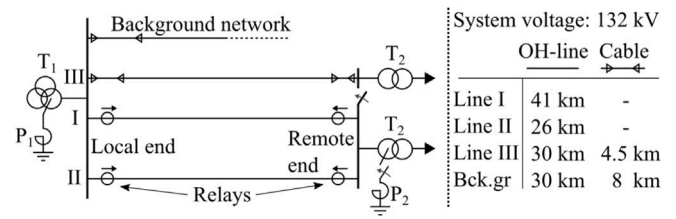Eq. (5) shows that the residual currents measured on lines A and B may become zero at certain fault locations, even in a network with several feeders. These fault locations are referred to as crossover points due to the fact that the polarity of the measured current transient will change from positive to negative in these points, and relays based on measuring this transient will therefore change their direction indication between forward and reverse as well. Furthermore, as the magnitude of the measured transient approaches zero, the relays may encounter problems in detecting the fault altogether when the fault is located close to this crossover point.

The point where either $3i_{0,A}$ or $3i_{0,B}$ becomes zero depends on the relative size of the ring compared to the background network and will occur for $3i_{0,A}$ when $R = m \cdot C_R/C_T$. Furthermore, if the ring is relatively large compared to the background network, this point is moved closer to the middle of the ring, and it can thus be imagined that both currents will be difficult to measure at certain fault points. In the special case of a single ring network ($C_R = C_T$), for instance in the case of a two-feeder network operated as a single ring, both $3i_{0,A}$ and $3i_{0,B}$ can become zero for the same fault location. The current measured at the remote end bus will also have its crossover point according to (6).

To be able to evaluate (5) and (6), the parameter m must be known. In the special case of a homogeneous ring, m is known to be exactly 0.5 due to the ring appearing identical seen from either main bus terminals of the ring. An analytical expression for the calculation of m has not been found, but it is understood to be governed by the distribution of capacitance around the ring. The formulae given in [19], used to describe a similar division of fundamental frequency zero-sequence currents, could serve as a starting point for deriving an analytical expression. In practice, however, the best way to locate the crossover points in a complex network would be to rely on simulations, seeing as analytical formulae quickly become difficult to derive when the network topology is changed from the one in Fig. 1. The purpose of deriving the formulae in this paper is to allow for a comparison between theory and practice using physical relays in a laboratory setup, which is presented in the next section.

3. Laboratory testing

3.1. Test network modeling

The results presented in this paper are based on simulations generated from the test network shown in Fig. 3, modeled using ATPDraw. The network is a radial network where two of the feeders have been connected to form a ring. Note that the illustration in Fig. 3 is compact, and feeders I and II are assumed far enough apart to be uncoupled. A third feeder can be connected in parallel to the ring, and the compensation can be divided among two different ASCs. This topology is not based on a real network, but it is first and foremost intended to facilitate a comparison between the actual location of the crossover points and the theoretical locations predicted by (5) and (6). See Table 1 for detailed model data.

3.2. Relay settings

The four relays (manuals [14–17]) under investigation are for the sake of confidentiality referred to as relays A–D:

- Relay A: Analog earth fault relay. The simplest relay of the four considered, with pickup level for transient current and fundamental frequency voltage being the only required settings. The relay is based on detecting transients in the zero-sequence current and voltage and comparing their polarities to determine the direction to fault. The relay manual refers to the charging transient as basis for the operating principle, and the transient measurement circuits are centered at 200 Hz.
- Relay B: Analog earth fault relay with the same basic operating principle as Relay A, also citing the charging transient as basis for its operating principle. According to the manual, the transient measurement circuits filters out the fundamental frequency component, and the measurement circuits for the current transients filters out transients above 3 kHz as well. The pickup level for current transient at 1 kHz and for the fundamental frequency voltage can be set by the user. Additionally, relay B allows for more detailed settings than Relay A, such as filter frequency, length of time window for detection of current and voltage transients, as well as delays related to resetting and tripping.
- Relay C: Numerical IED with multiple earth fault functions, where only the transient earth fault function is being tested. This function is also based on the transient charging process that takes place during earth faults, but as opposed to relay A and B, this function also considers the fundamental frequency in addition to the higher frequency transients. According to the manual, this function is based on the energy in the zero-sequence system, citing that the charging process consists of a transfer of energy between the faulty feeder and the surrounding network. This zero-sequence energy is computed through integration and summation of phasors at several frequencies. The relay allows for setting of $3V_0$ and the integrated $3I_0$-current trigger levels, along with detailed settings of proprietary parameters. This relay also allows separate trigger levels for forward and reverse faults.
- Relay D: Numerical IED with multiple earth fault functions, where only the transient earth fault function is being tested. Similar to relay C, this function is based on the energy in the zero-sequence system, which is computed directly in the time domain. The relay manual for relay D contains less information on the signal processing and filtering, but it indicates that relay D also makes use of the fundamental frequency in addition the higher frequencies, just as relay C does. The relay allows for setting of $3I_0$ and $3V_0$ trigger levels, along with detailed settings of proprietary parameters.

All the four relays require the same two measurements, $3I_0$ and $3V_0$. Relays A and B both refer directly to the charging transient discussed previously as basis for their operation. Relays C and D are based on zero-sequence energy, although they have different ways of implementing it. While the charging transient is part of this operating principle, relays C and D also incorporate more of the information contained in the transient period in their operation. The four relays thus represent two generations of relays utilizing two distinctly different operating principles. Whereas relays A and B are found in many Norwegian networks today, relays C and D are likely to be used increasingly in new substations.

Although the relays utilize similar operating principles, the implementation and configuration of each relay is unique. The only comparable setting is the pickup threshold for the fundamental frequency voltage $3V_0$, which is set to ensure fault detection for all the relays. The four relays all have a setting for the current threshold as well, although it has different interpretations for each relay. In the case of relays A and B, the current threshold has a recommended value based on network data and the CT-ratio used. This parameter is therefore set according to the recommendations in their respective manuals. All other proprietary settings are set according to the manuals unless otherwise specified. Relays C and D have current thresholds that

Table 1
Test network data.

OH-lines	Phase conductors: radius 4.07 mm (inner) and 12.03 mm (outer), R_{DC} = 0.1115 ohm/km, 4.5 m spacing, plane geometry, tower height 11 m, 4.3 m sag. Ground conductors (x2): radius 1.45 mm, R_{DC} = 0.8 ohm/km, 4.5 m spacing, plane geometry, tower height 13 m, 4.3 m sag. Transposed lines, skin effect, JMarti-model. No coupling between feeder I and II. G_0 = 44.33 nS/km added manually.
Cables	Three single-phase cables in ground, depth 1 m, transposed. Core radii 8 mm (inner) and 17.35 mm (outer), sheath radii 32.15 mm (inner) and 33 mm (outer), cable radius 41 mm, semi.cond. layer w/ thickness 1 mm between core and sheath, conductor resistivity 2.651E−8 Ωm, relative permittivity of insulation 2.3. Modeled using JMarti. Asymmetry: 3.3 nF/km and 6.6 nF/km added to C_0 in phases b and c, respectively.
Transformers	T1: 250/250/80 MVA 400/132/12.5 kV Yyd1 T2: 50 MVA 132/22 kV Yd11
Loads	3-phase 10 MVA constant impedance loads. Power factor 0.9 lagging.
ASC	I_{nom} = 295 A (10% over-compensated). Parallel resistors R_p = 50 kΩ represent losses in P1 and P2.
CTs and VTs	$3I_0$ CTs 600/5A, $3V_0$ VTs 228/0.11 kV. Sampled at 10 kHz.
Fault	R_f = 100 Ω, inception angle approximately 40°.
Other	Software: ATPDraw version 7.2p11, simulation timestep Δt = 1 μs, ground resistivity 100 Ωm.

are related to either the CT secondary current or as a percentage of some base value. Relay C limits the current threshold downwards to some percentage of base value, typically the CT primary value, while relay D allows setting the threshold to zero. However, the manual of relay D states that this threshold should perhaps be increased in meshed networks according to user experience.

In either case, default pickup thresholds of relays C and D cannot be readily obtained from their manuals. Furthermore, the correct operation of all four relays is closely related to the quality of the measurements they receive. In reality, measurement noise will be present, and an appropriate CT-ratio must be used to give the relays optimal conditions. In this paper it is primarily the fault direction indication which is of interest to study, and the relays are therefore set to be very sensitive. Discussion of any observed issues pertaining to sensitivity of the relays will therefore be limited to a qualitative level.

3.3. Laboratory setup

Signals of $3I_0$ and $3V_0$ on Comtrade format are generated using ATPDraw's Comtrade block sampling at 10 kHz, where the fault records are obtained running sequential simulations with varying parameters. The Advanced TransPlay feature in Omicron CMC 356 is used to play the Comtrade files to the relays [21].

All the relays are capable of outputting binary signals to indicate both forward and reverse faults, and these signals are monitored to determine the location of the crossover points. The binary signals are synchronized in time with the signal played back by the relay tester with the setup shown in Fig. 4, and all binary signals are controlled to make sure that they coincide with the fault.

4. Results

4.1. Location of crossover points

Faults are applied in sequence at evenly distributed locations around the ring consisting of feeder I and feeder II in the network in Fig. 3 to investigate the location of the crossover points. Feeder III is assumed to be operated radially, and ASC P2 is disconnected. Based on the charging transient alone, the theoretical location of these points can be
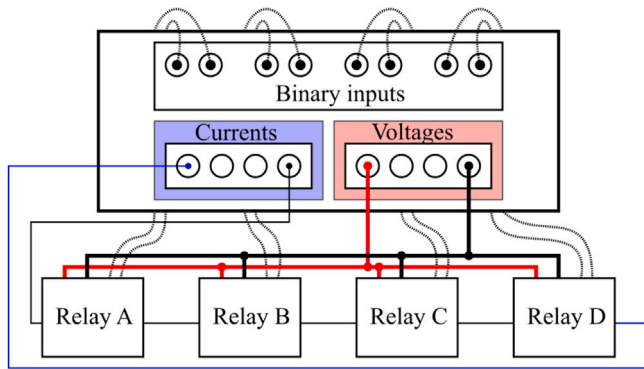
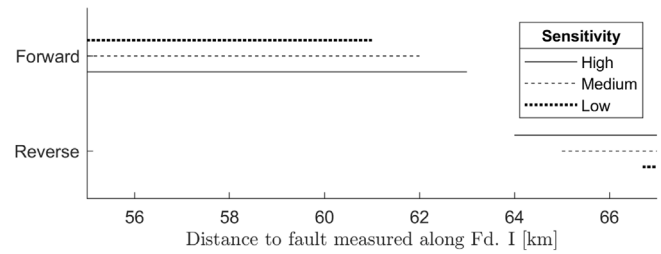**Fig. 4.** Lab setup for testing multiple relays at once using the Omicron CMC 356 [21].

Fig. 5. The crossover point of relay A turns into a crossover region as the relay sensitivity is decreased.

Fig. 6. The current $3I_0$ as measured on the local end of Fd. I for various fault locations.

estimated using (5) and (6). The parameters M and m are determined as follows: M describes the per unit distance to the remote end bus as $M = 41\text{ km}/67\text{ km} = 0.612$, and $m = 0.5$ is assumed because the ring is homogeneous with only overhead lines. For the four relays on the ring, these theoretical locations are shown in Table 2 along with the observed crossover points for the four relays.

Using standard settings as recommended by the relay manufacturers, Relay A managed to detect the fault in all the fault locations. Relay D managed to detect all the faults as well, likely due to the fact that this relay both allows and recommends a very low current threshold. Relay C behaves differently as its sensitivity threshold is related to whatever current level is selected as its base value. The selection of this base value is up to the user, but with a sufficiently low value Relay C can also be made to be very sensitive. Relay B was the least sensitive, and its minimum allowable current threshold setting was used to determine its crossover point location. Furthermore, it was observed that the remote end relays had much poorer operating conditions than the local end relays did, requiring the output from the relay tester to be twice as high in order to determine the crossover point location. This demonstrates that a single setting for all the relays in the network, as suggested in the manuals of both relays A and B, is not advisable.

The results show that the relays have their crossover points close to the theoretical values, but that there is some variation. This may in part be due to differences in the operating principles, and partly due to the fact that faults close to the crossover point represent very challenging conditions for the relays. The precise locations of the crossover points were therefore difficult to determine accurately in the laboratory setup, as the observed locations of the crossover points shifted slightly in some instances (at most ± 4 km) when the tests were conducted with different relays settings and CT-ratios.

In addition to the results in Table 2, the impact of adding feeder III in parallel was investigated. This shifted the locations of the crossover points for all the relays, as would be expected from the theoretical discussions in Section 2.

4.2. Crossover regions

As discussed previously, two things occur in the crossover points: (1) the polarity of the charging transient changes, and (2) the magnitude of the charging transient goes to zero, as was shown in [18]. Although the transition from forward to reverse happens in the crossover point, the magnitude gradually decreases in the area around the crossover point. As a result, the relays may fail to detect faults in the region around the crossover point when less sensitive settings are used. Therefore, the crossover points would actually appear as crossover regions in reality. Fig. 5 illustrates this for Relay A, and similar results could be produced for the other relays as well. The relay was fed with currents of 30%, 25% and 15% magnitude to emulate a high, medium and low sensitivity setting. Note that because the relay was set less sensitive than its recommended settings. i.e., its pickup threshold was set higher than recommended, the crossover point in Fig. 5 is actually shifted slightly from the value in Table 2. The sensitivity of the relay and the approach used to locate the crossover point thus both impact the observed crossover point location, further illustrating that the exact crossover point location is difficult to determine. This was observed to a varying degree for all the four relays, with relay A showing the largest shift.

Fig. 5 illustrates how the crossover point turns into a crossover region as the sensitivity of the relay is decreased, and faults in this region are not detected by the relay. Fig. 6 shows the time domain signal obtained at the local end relay on feeder I. It illustrates that the initial transient is drastically reduced as the fault is moved farther away, and the polarity shift can also be observed to take place towards the other end of the ring corresponding to the 67 km curve. The magnitude of the fundamental frequency component is also visibly reduced for faults far away.

4.3. Impact of the fundamental frequency component

Dividing the compensation in the network evenly among ASC P1 and P2 further impacted relays C and D, whereas relays A and B were unaffected. Relays A and B only utilize frequencies above the fundamental frequency, for which the network appears ungrounded. Changing or moving the ASCs in the network will therefore not affect
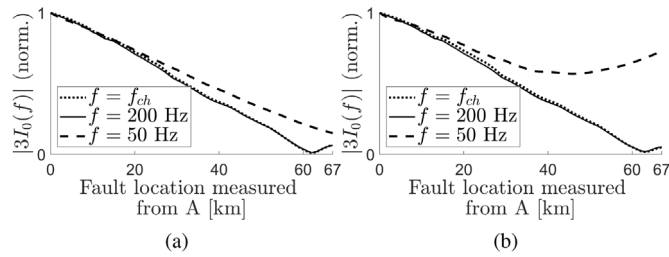
Table 2
Theoretical and observed crossover points the test network.

Relay pos.	Local end		Remote end	
	Fd. I	Fd. II	Fd. I	Fd. II
Crossover points - (km/*p.u.*)				
(measured from local end bus in clockwise direction around the ring)				
Theoretical crossover point	63.6/*0.95*	3.4/*0.05*	0.8/*0.01*	0.8/*0.01*
Relay A	58.5/*0.87*	8.5/*0.13*	1.5/*0.02*	1.5/*0.02*
Relay B	62.5/*0.93*	4.5/*0.07*	1.5/*0.02*	1.5/*0.02*
Relay C	65.5/*0.98*	1.5/*0.02*	0.5/*0.01*	0.5/*0.01*
Relay D	65.5/*0.98*	1.5/*0.02*	0.5/*0.01*	0.5/*0.01*

Fig. 7. Normalized magnitudes of the charging transient, 200 Hz and 50 Hz components in $3I_0$ during the first 20 ms of the fault, measured at local end Fd. I, in the case of one (a) or two (b) ASCs in the network.
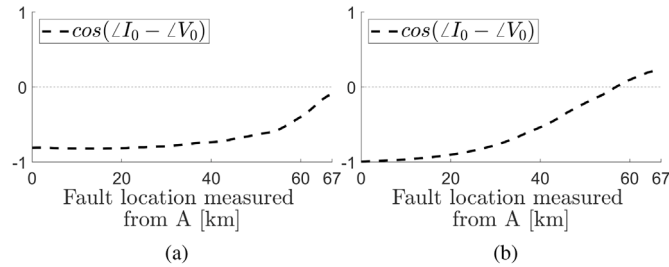

Fig. 8. 50 Hz zero-sequence power factor during the first 20 ms of the fault, measured at local end Fd. I, in the case of one (a) or two (b) ASCs in the network.

these relays. Relays C and D, however, both make use of the fundamental frequency, and their crossover points are therefore dependent on the location of the ASCs in the network. Fig. 7 shows how the magnitudes of the charging transient, the 200 Hz and 50 Hz component of $3I_0$ varies with fault location in these two scenarios, and it is clear that relays dependent on the 50 Hz component will be affected by adding the second ASC.

The addition of P2 not only affects the magnitude of the fundamental frequency component, but also the direction indication based on it. Relays C and D both rely the zero-sequence active energy as part of their operation, and Fig. 8 show that the fundamental frequency active power always indicates a forward fault ($cos(\phi_0) < 0$) in the case of a single ASC, while the addition of P2 changes this. Relays C and D do however not exhibit the exact same responses (the addition of P2 shifted the crossover points of relays C and D in opposite directions), demonstrating that they each have a distinct variation of the energy-based operating principle. The formulae presented in Section 2 only account for the behavior of the charging transient, and therefore do not accurately capture the behavior of relays C and D. This will require a separate study of the fundamental frequency component as well as the relays' weighting of the different frequencies, which is outside the scope of this paper.

4.4. Challenges for protection

Assuming that the relays could be set as sensitive in reality as they were during this test, the data in Table 2 show that misoperation could occur. Fig. 9 illustrates the situation: The remote end relay on feeder II see faults on the first 0.5–1.5 km of feeder I as forward faults, whereas the remote end relay on feeder I see them as reverse faults. As a result, no pair of relays on the ring can determine the fault to be between them. Instead, a network operator would have two options in this case: (1) increase the pickup threshold of the relays and only rely on the local end relays to determine the fault location, or (2) divide feeder I in two shorter segments equipped with another pair of relays.

Because the different relays are affected differently by the presence of ASCs, a network with a mixture of different relays could result in another more critical type of misoperation. Consider the situation in
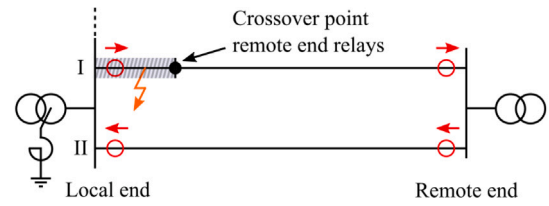

Fig. 9. The shaded region shows fault locations with inconclusive relay responses.
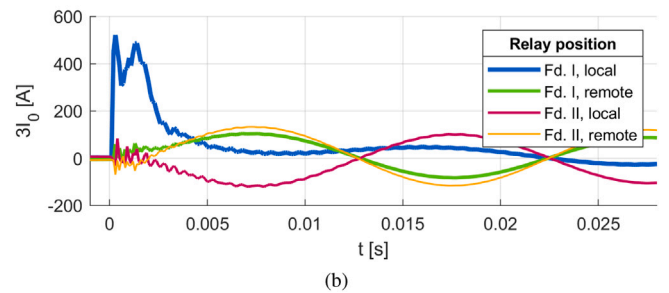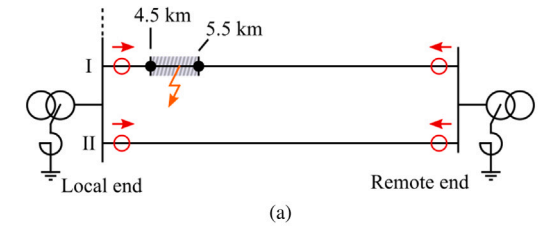

Fig. 10. Faults in the shaded region in (a) appear as a forward fault on both lines. Current magnitudes in (b) clearly indicate a fault on Fd. I (actual fault location is 5 km from the local end on Fd. I).

Fig. 10(a), where the compensation is divided evenly among P1 and P2. Assume that the relays in the local end substation are of type B, whereas the remote end substation is equipped with type D relays. Table 3 shows the location of the crossover points in this configuration. Because the crossover point of the remote end relay on feeder II is located farther out on feeder I than the crossover point of the local end relay on feeder II, all four relays see faults in the shaded region as forward faults. The local-end relay on feeder II must in this case have its pickup threshold increased to avoid this situation.

The actual magnitude of the transients will depend on several factors such as inception angle and fault resistance, and therefore it is difficult to relate the magnitude to any particular fault location. However, if the magnitudes of the currents measured by each relay had been available for comparison in the previous example, the fault could easily have been determined to be on feeder I. The maximum recorded value of $3I_0$ in the local end relay on feeder I is much higher than at the other three relays, as shown in Fig. 10(b), indicating that the fault could not possibly be located on feeder II.

5. Discussion

Testing relays based on simulations is a challenge, as replicating both the earth fault transients as well as the fundamental frequency components accurately is difficult.

Firstly, the relay tester must reproduce the waveforms accurately, which may be difficult for very fast transients. Furthermore, the Omicron is limited to playing back 10 kHz, although this should be more than any of the relays require.

Secondly, the use of the frequency dependent line model does not perfectly replicate both the fundamental frequency (50 Hz) and the fault transients (0.2–2 kHz). This is however only of concern for relays

Table 3
Observed crossover points for relay B and D when ASC P2 is connected.

Relay pos.	Local end		Remote end	
	Fd. I	Fd. II	Fd. I	Fd. II
	Crossover points - (km/*p.u.*) (measured from local end bus in clockwise direction around the ring)			
Relay B	62.5/*0.93*	4.5/*0.07*		
Relay D			64.5/*0.97*	5.5/*0.08*

C and D, for which the impact of the fundamental component is only discussed on a qualitative level. Furthermore, the effect of CT and VT accuracy and noise is not implemented in these tests, and the very sensitive relay settings required in these tests may not be realistic to implement in reality to avoid false alarms during other network events. It may also be the case that the set sensitivity of the relays should be deliberately reduced to avoid the simultaneous operation of too many relays in the network and to reduce the risk of misoperation due to poor conditions near the crossover points.

Finally, it is noted that the topology of the test network is intentionally simple to enable derivation of the analytical formulae which could be compared against laboratory tests. In reality, such a ring-network would likely have many lateral branches which complicates the process of estimating the location of the crossover points. The fact that crossover points would exist in any type of non-radial network is obvious, and in complex networks their location may be more efficiently determined through simulations.

6. Conclusion

Transient earth fault relays (TEFRs) are frequently applied to non-radial resonant grounded networks, but they are susceptible to issues related to both sensitivity and polarity. This paper has presented and verified a theoretical approach for estimating the location of crossover points for relays based on the charging transient, i.e. fault locations in which a relay will change its direction indication between forward and reverse, and tested four different commercially available TEFRs in a laboratory setup. The important conclusions and scientific contributions are as follows:

- Crossover points were found in the predicted locations, and b polarity swap and sensitivity issues were observed there, showing that the theoretical approach for understanding crossover points is correct. This approach can therefore be used to understand relay behavior in other networks as well, although simulations likely are more efficient in the case of complex topologies.
- The location of the crossover points for the modern relays based on zero-sequence energy are also influenced by the fundamental frequency component, which in turn is affected by network topology and the placement of arc suppression coils in the network. This is not accounted for in the analytical formulae presented in this paper, and future work should focus on extending the theory to encompass this.
- Because the location of the crossover points depend on the network topology, and as different relay locations can have significantly different operating conditions with respect to expected current magnitudes, static and system-wide settings for all relays in the network, as suggested in some relay manuals, is not advisable. Rather, each relay location should be analyzed separately, and this analysis should take into account all the possible network topologies to ensure the desired behavior during faults.
- All the TEFRs must deal with the lack of a clear forward/reverse orientation in a loop, and due to the lack of a distance element in TEFRs, the evaluation of relay responses with respect to this issue becomes difficult. Ring-operation of distribution networks is particularly challenging to protect with TEFRs when one or more

relays have their crossover points on the protected line itself. Knowledge of the likely crossover regions and comparison of the current magnitudes of relays in the system could however be used to aid the network operator when assessing the relay responses.

CRediT authorship contribution statement

Thomas Treider: Conceptualization, Methodology, Software, Formal analysis, Investigation, Data curation, Writing – original draft, Writing – review & editing, Visualization. **Hans Kristian Høidalen:** Methodology, Software, Writing – review & editing.

Declaration of competing interest

The authors declare that they have no known competing financial interests or personal relationships that could have appeared to influence the work reported in this paper.

Data availability

The authors do not have permission to share data.

References

[1] X. Zhang, B. Xu, Z. Pan, P. Wei, Study on single-phase earthed faulty feeder selection methods in non-solidly grounded systems, in: 2008 3rd Int. Conf. Elect. Utility Deregulation and Restructuring and Power Techn., 2008, pp. 1836–1840.

[2] E. Bjerkan, Efficient fault management using remote fault indicators, in: CIRED 2009 - the 20th Int. Conf. Exhib. Electricity Distribution - Part 1, 2009, pp. 1–4.

[3] A. Wahlroos, J. Altonen, Performance of novel neutral admittance criterion in MV-feeder earth-fault protection, in: CIRED 2009 - 20th Int. Conf. Exhib. Electricity Distribution - Part 1, 2009, pp. 1–4.

[4] T. Henriksen, Faulty feeder identification in high impedance grounded network using charge–voltage relationship, Electr. Power Syst. Res. 81 (9) (2011) 1832–1839.

[5] M. Loos, S. Werben, M. Kereit, J.-C. Maun, Detection of single phase earth fault in compensated network with C0 estimation, in: CIRED 2013 - 22nd Int. Conf. Exhib. Electricity Distribution, 2013, pp. 1–4.

[6] K. Pandakov, H.K. Høidalen, S. Trætteberg, An additional criterion for faulty feeder selection during ground faults in compensated distribution networks, IEEE Trans. Power Deliv. 33 (6) (2018) 2930–2937.

[7] J. Rios Penaloza, A. Borghetti, F. Napolitano, F. Tossani, C. Nucci, Performance analysis of a transient-based earth fault protection system for unearthed and compensated radial distribution networks, Electr. Power Syst. Res. 197 (2021) 107306.

[8] M. Abdel-Fattah, M. Lehtonen, Transient algorithm based on earth capacitance estimation for earth-fault detection in medium-voltage networks, IET Gener., Transmiss. Distrib. 6 (2) (2012) 161–166.

[9] G. Druml, P. Stachel, S. Gebhard, W. Leitner, O. Skrbinjek, G. Achleitner, U. Schmidt, P. Schegner, New method for measuring the earthfault-distance in compensated and isolated networks, in: CIRED 2021 - the 26th Int. Conf. Exhib. Electricity Distribution, 2021, pp. 1416–1419.

[10] G. Druml, P. Stachel, W. Leitner, O. Skrbinjek, U. Schmidt, P. Schegner, Results from the new method for measuring the earthfault-distance in compensated and isolated networks, in: 16th Int. Conf. Develops. Power Syst. Protection, DPSP 2022, 2022, pp. 13–18.

[11] J.D. Rios Penaloza, A. Borghetti, F. Napolitano, F. Tossani, C.A. Nucci, Performance analysis of a communication-supported earth fault protection system of medium voltage loop and meshed networks, in: 2018 IEEE Int. Conf. Environ. and Elect. Eng. and 2018 IEEE Ind. and Commercial Power Sys. Europe (EEEIC / I&CPS Europe), 2018, pp. 1–6.

[12] J.D. Rios Penaloza, A. Borghetti, F. Napolitano, F. Tossani, C.A. Nucci, A new transient-based earth fault protection system for unearthed meshed distribution networks, IEEE Trans. Power Deliv. 36 (5) (2021) 2585–2594.

[13] T.A. Zerihun, T. Treider, H. Taxt, L.B. Nordevall, T.S. Haugan, Two novel current-based methods for locating earth faults in unearthed ring operating MV networks, Electr. Power Syst. Res. 213 (2022) 108774.

[14] Siemens AG, 7SN600 Transient Earth-Fault Relay: Instruction Manual, Oct. 2011, Nuremberg, Germany, 2011.

[15] ABB Relays AB, Type RXPG 4 Transient Ground-Fault Relay, B03-3110E, Västerås, Sweden, 1989.

[16] Hitachi Energy Sweden AB, "Average Power Transient Earth Fault Protection, APPTEF," in Relion 670 Series: Line differential protection RED670, Version 2.2 ANSI Technical Manual, Västerås, Sweden, 2022.

[17] Siemens AG, "Directional Transient Ground-Fault Stage," in SIPROTEC 5, Generator Protection, Manual C53000-G5040-C027-9, 04.2021, Nuremberg, Germany, 2021.

[18] T. Treider, B. Gustavsen, H.K. Høidalen, Analysis of transient earth fault protection in meshed resonant grounded networks, in: 16th Int. Conf. Develops. Power Syst. Protection (DPSP 2022), 2022, pp. 1–6.

[19] R. Willheim, R. Waters, Neutral Grounding in High-Voltage Transmission, Elsevier, New York, NY, USA, 1956, pp. 198–200.

[20] T. Welfonder, Localisation de défauts monophasés dans les réseaux de distribution à neutre compensé (Ph.D. thesis), Grenoble INPG, 1998.

[21] Omicron, CMC 356 : User Manual, Omicron electronics GmbH.